Article

Effect of Thermal Treatment of Symmetric TiO₂ Nanotube Arrays in Argon on Photocatalytic CO₂ Conversion

Timofey Savchuk [1,2], Ilya Gavrilin [1], Andrey Savitskiy [1,3], Alexey Dronov [1], Daria Dronova [1], Svetlana Pereverzeva [1,3], Andrey Tarhanov [1], Tomasz Maniecki [2], Sergey Gavrilov [1] and Elizaveta Konstantinova [4,*]

1   Institute of Advanced Materials and Technologies, National Research University of Electronic Technology—MIET, Bld. 1, Shokin Square, Zelenograd, 124498 Moscow, Russia
2   Institute of General and Ecological Chemistry, Lodz University of Technology, 90-924 Lodz, Poland
3   Scientific-Manufacturing Complex "Technological Centre", Zelenograd, 124498 Moscow, Russia
4   Physics Department, M.V. Lomonosov Moscow State University, Leninskie Gory 1-2, 119991 Moscow, Russia
*   Correspondence: liza35@mail.ru; Tel.: +7-(916)-887-49-14

Abstract: Symmetric titania nanotube arrays (TiO₂ NTs) are a well-known photocatalyst with a large surface area and band edge potentials suitable for redox reactions. Thermal treatment of symmetrical arrays of TiO₂ nanotubes in argon was used to change the carbon content of the samples. The influence of the carbon content in the structure of symmetrical TiO₂ NTs on their photoelectrochemical properties and photocatalytic activity in the conversion of CO₂ into organic fuel precursors has been studied. The structure, chemical, and phase composition of obtained samples were studied by X-ray analysis, Raman spectroscopy, and SEM with energy dispersive analysis. It is established that carbon-related defects in the samples accumulate electrons on the surface required for the CO₂ conversion reaction. It has been shown for the first time that varying the carbon content in symmetric TiO₂ NTs arrays by annealing at different temperatures in argon makes it possible to control the yield of methane and methanol in CO₂ conversion. It is revealed that too high a concentration of carbon dangling bonds promotes the growth of CO₂ conversion efficiency but causes instability in this process. The obtained results show a high promise of symmetric carbon-doped TiO₂ NTs arrays for the photocatalytic conversion of CO₂.

Keywords: symmetric TiO₂ nanotube arrays; CO₂ conversion; photocatalysis; carbon

1. Introduction

Climate change due to increasing greenhouse gas (CH₄, CO₂) concentrations has attracted increasing attention from the scientific community [1]. Photocatalytic conversion of CO₂ to hydrocarbon fuel precursors may be one approach to the transition to carbon neutrality energy [2,3].

TiO₂-based photocatalysts have attracted much attention for the CO₂ conversion process because of their chemical and photocorrosion stability, and also low cost [4–6]. Symmetric titania nanotube arrays (TiO₂ NTs) are a well-known photocorrosion-resistant nanomaterial for use in photocatalytic processes due to their high specific surface area and suitable band edge potentials [7,8]. However, TiO₂ NTs are not photoactive in the visible wavelength range, which hinders the use of this material as a photocatalyst.

Today, there are several approaches to increasing the photocatalytic activity of titanium oxide in the visible wavelength range. It was shown that to expand the absorption spectrum of titanium oxide or other semiconductors, and increase the lifetime of photogenerated charge carriers, can use the formation of heterojunctions by modifying the surface with metals nanoparticles Pd, Pd₂Cu, Pt, Ag [9–11], semiconductors CuO, TiO₂, WO₃, Fe₂O₃ [12,13], various modifications of carbon [14,15] and perovskites nanoparticles [16,17]. It is also well known that the thermal treatment of titanium oxide in oxygen-free atmospheres (H₂, Ar,

vacuum) promotes the formation of point defects (oxygen vacancies) in the oxide structure and on its surface, changing the concentration of which can control the photocatalytic activity of titanium oxide in the visible range [18]. It was also shown that doping with non-metals S, C, and N [19,20] makes it possible to expand the absorption spectrum of titanium oxide due to the formation of energy levels in the band gap of the semiconductor. In turn, the modification of titanium oxide by carbon can solve three symmetric problems for photocatalysis applications: reduce the electrical resistance, improve the separation of photogenerated charge carriers and increase the photoactivity of the material in the visible light range [21–24].

One approach to carbon modification of TiO_2 NTs arrays can be thermal treatment in inert atmospheres of nanotubes obtained in ethylene glycol-based electrolytes [25–28]. High-ordered symmetric arrays of titania nanotubes with a multi-wall nanotube structure [29] and oxide layer thicknesses ranging from one to several hundred micrometers can be obtained in such electrolytes [30]. The inner layer (IL) of a nanotube, is a mixture of solvolysis products of dissolved in water complex $[TiF_6]^{2-}$ and ethylene glycol. During thermal treatment in oxygen-free atmospheres, the IL of a nanotube can be a source of carbon for material modification [26]. We have previously shown that carbon centers on the surface of the IL saved after thermal treatment in the air can enhance the conversion efficiency of CO_2 [31]. As far as we know, the works devoted to the study of symmetric TiO_2 NTs arrays modified by carbon through thermal treatment in inert atmospheres pay attention to the electrochemical properties of the material for supercapacitors or the study of photoactivity by photoelectrochemistry and decomposition of organic dyes. In turn, thermal treatment in such atmospheres should help preserve more carbon in the material, potentially leading to high material activity in photocatalytic CO_2 conversion. However, no works devoted to the study of the photocatalytic properties of carbon-modified symmetric TiO_2 NTs arrays in the process of CO_2 conversion have been previously presented.

In the present work, we investigated the influence of thermal treatment conditions in argon on structure, chemical and phase composition, and photocatalytic properties of carbon-modified symmetric titania nanotube arrays during carbon dioxide conversion in the presence of water vapor.

2. Materials and Methods

Samples of symmetric titania nanotube arrays were obtained by electrochemical oxidation of titanium foil (99.7%). Electrolyte used: ethylene glycol, 0.3 g NH_4F, 2 mL H_2O per 100 mL electrolyte volume. Anodizing was performed in a horizontal thermostatically controlled cell at 20 °C in two stages. The first stage lasted 30 min, and then the formed nanotube layer was removed from the surface of the foil. The second stage lasted 1 h, after which the sample was washed in ethyl alcohol and dried in an air stream. The anodized area of the samples was 7 cm^2. The geometric-specific surface area of the samples is 0.0054 m^2/cm^2 corresponding with previously published data [31].

The as-prepared samples are not photocatalytic active due to a non-symmetric amorphous oxide structure (TiO_x). The samples were subjected to thermal treatment for crystallization in an argon flow of 100 mL/min at 1.1 atm overpressure at different temperatures (300, 400, 550 °C) for 1 h. A sample annealed in air at 450 °C for 1 h was prepared as a comparison sample (Air 450). The thermal treatment in an argon inert atmosphere was used to pyrolyze the organic content in the as-prepared samples and preserve carbon during heating.

The phase transformations during heating of symmetric TiO_2 NTs samples in an argon atmosphere (purity 99.999%) were investigated by differential thermal analysis (DTA) and thermogravimetric analysis (TGA) on the Setsys TG-DTA 16 with simultaneous registration of pyrolysis products by mass spectrometric analysis. The analysis was performed in the temperature range of 25–700 °C at a heating rate of 10 °C/min. The samples for analysis were prepared by scraping the oxide layer from the titanium substrate.

The morphology and sample composition were studied by scanning electron microscopy (SEM) using a Helios G4CX (Thermo Fisher Scientific, Waltham, MA, USA) scanning electron microscope equipped with an EDS attachment (EDAX Octane Elite Super).

Spectra of diffuse light reflection from the samples were recorded on an SF-56 spectrometer (OKB-Spectr, St. Petersburg, Russia) in a spectral range from 300 to 650 nm.

Raman spectra were obtained on a LabRAM HR Evolution Raman spectrometer (manufactured by Horiba) using a Melles Griot 05-LHP-928 helium-neon laser at the operating wavelength of 633 nm. X-ray diffractometer Rigaku MiniFlex XRD was used to analyze the obtained symmetric TiO_2 NTs samples.

The photoelectrochemical properties of the obtained samples were studied in a 0.1 M Na_2SO_4 solution with a platinum counter electrode and a silver chloride reference electrode (3 M KCl). A 150 W xenon lamp NEWPORT (Ozone Free) 6255 was used as the light source, the incident light intensity on the sample was 100 mW/cm^2. For measurements in the visible light range, an optical filter was used to cut off radiation with a wavelength of less than 430 nm. Photoelectrochemical measurements were performed using an AutoLab PGSTAT302N potentiostat. Photocurrent measurements were performed at a zero volt constant potential vs. Ag/AgCl with alternating switching a light to record the photoresponse of the sample. The voltammetric characteristics of the samples were obtained in the potential range from −0.6 to 1.6 V vs. Ag/AgCl at a sweep rate of 10 mV/s.

Incident photon-to-electron conversion efficiency was evaluated by photocurrent spectroscopy based on the ZOLEX photoelectrochemical measurement complex. A xenon lamp with a total power of 500 watts was used as the light source. The photocurrent was measured in the range of 300 to 500 nm in 25 nm increments and at 0 V applied potential vs. Ag/AgCl. Quantum efficiency was calculated according to Formula (1) [32]:

$$IPCE = \frac{j_{ph(\lambda)}}{P_{(\lambda)}} * \frac{1240}{\lambda} \tag{1}$$

$$j_{ph} = \left| \frac{\left(I_{light} - I_{dark} \right)}{S} \right| \tag{2}$$

where j_{ph} is the difference between the recorded values of current density in the dark and in the light at the selected wavelength ($\mu A \cdot cm^{-2}$), λ—the wavelength at which the measurement was made (nm), $P(\lambda)$ is the power of incident light at the selected wavelength ($\mu W \cdot cm^{-2}$), S is the sample area, (cm^2).

The process of photoinduced conversion of CO_2 was performed under the following conditions: reaction temperature 30 °C, relative humidity ~5%, total CO_2 (99.999%) gas flow rate—1.2 mL/min. Before measurements, the samples were placed in the reactor in a helium stream (99.999%, flow rate—3 mL/min) with water vapor overnight (10 h) to remove air from the chamber. Firstly, the samples were illuminated (~2 h) in a stream of moist helium with a flow rate of 1.2 mL/min with the recording of photocatalytic reaction products to clean the surface from organic substances. Then the flow changes to CO_2 while maintaining the gas flow rate. The light irradiation was turned off after 4 h. Gas products were analyzed using a gas chromatograph with a flame ionization detector with an HP PLOT/Q capillary column.

3. Results and Discussion

3.1. Thermal Treatment Condition Determination

Figure 1 shows the results of differential scanning calorimetry and thermogravimetric analysis obtained together with the registration of pyrolysis reaction products. Molecules with masses 16, 18, 28, and 44 by mass spectrometry were recorded.
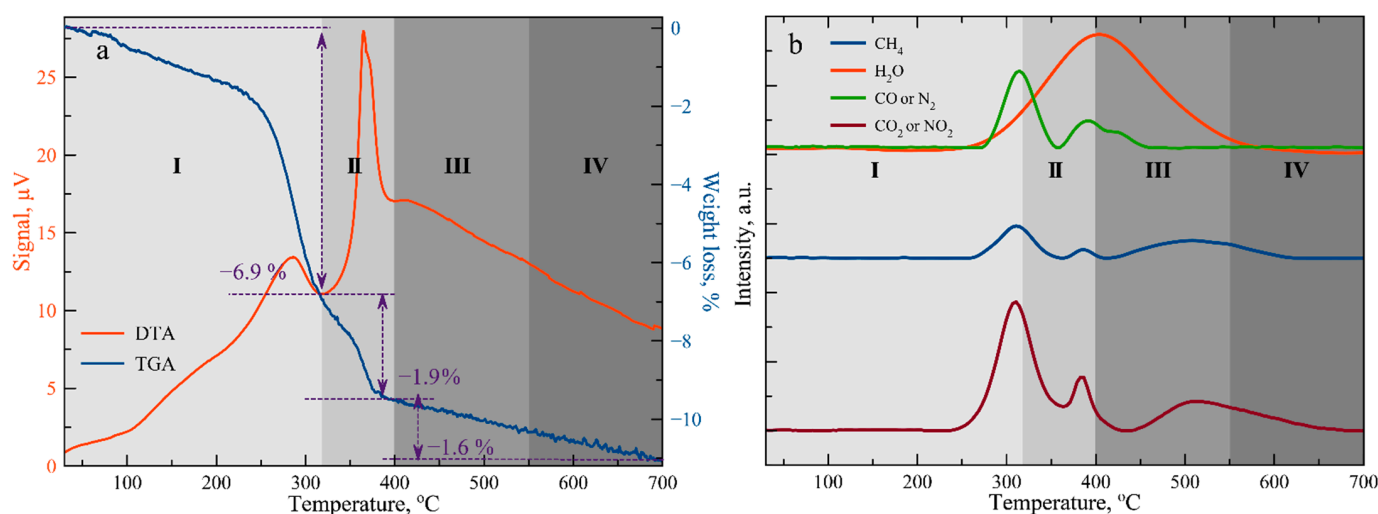
Figure 1. DTA-TGA dependences (**a**) and in situ registered mass spectra products (**b**) of a thermal decomposition process: I, II, III and IV are stages of the process.

Two exothermic peaks are observed in the process of heating the powder of amorphous samples in the argon flow. The first peak (at 280 °C) is accompanied by the greatest release of carbon monoxide or molecular nitrogen (CO, N_2), methane (CH_4) and carbon dioxide or nitrogen oxide (CO_2, N_2O). The release of products can be attributed to the pyrolysis of organic compounds and electrolyte residues (nitrogen source) (stage I) in the sample and the desorption of thermal reaction products from the material surface. This process is also accompanied by an extensive sample mass loss of about 5.6 wt.% in the temperature range of 220–330 °C. The second stage II is accompanied by further weight loss (about 1.9 wt.%) and crystallization of amorphous titanium oxide (TiO_x) occurs at 365 °C. Crystallization is accompanied by the re-registration of pyrolysis products, which can be attributed to the thermal decomposition of organics located at some depth of the surface layer of nanotubes. The plateau is observed at 400 °C on the DSC curve with a further decrease in signal intensity. At the same time in the temperature range from 450 to 650 °C the release of methane and carbon dioxide is observed. That effect can be attributed to the pyrolysis of more deeply retained products of ethylene glycol decomposition in the oxide volume (stage III). The mass loss when heating the sample in the temperature range from 380 to 700 °C was 1.6%. Finally, stage IV is associated with no release of any products or thermal effects, which can indicate removing residual organic matter from the material. Based on the data obtained, four temperature ranges were identified at which the greatest change in the structure and composition of the material occurs. The temperatures of isothermal treatment of the obtained samples of symmetric TiO_2 NTs arrays were chosen: 300, 400, and 550 °C to study the material properties at the boundaries of certain ranges. Carbon after pyrolysis is saved at 300 °C (stage I), but there is no crystallization of the structure. The material structure crystallizes and part of the carbon is retained at 400 °C (the boundary of stages II and III). The structure of the material is also crystalline and residual carbon could be removed at 550 °C (stage IV). The samples thermal treated in argon were designated as Arg 300, Arg 400, and Arg 550, respectively.

3.2. Morphology and Composition of Samples Characterization

Figure 2 shows SEM images of symmetric TiO_2 NTs arrays annealed in the air and argon stream.

The pore size of all obtained samples ranges from 40 to 90 nm. The thickness of the oxide layer does not change with temperature and annealing atmosphere ~5.6 μm.

The composition of obtained samples was also investigated by energy dispersive X-ray spectroscopy (EDS), and the summarized results of the analysis are presented in Table 1.
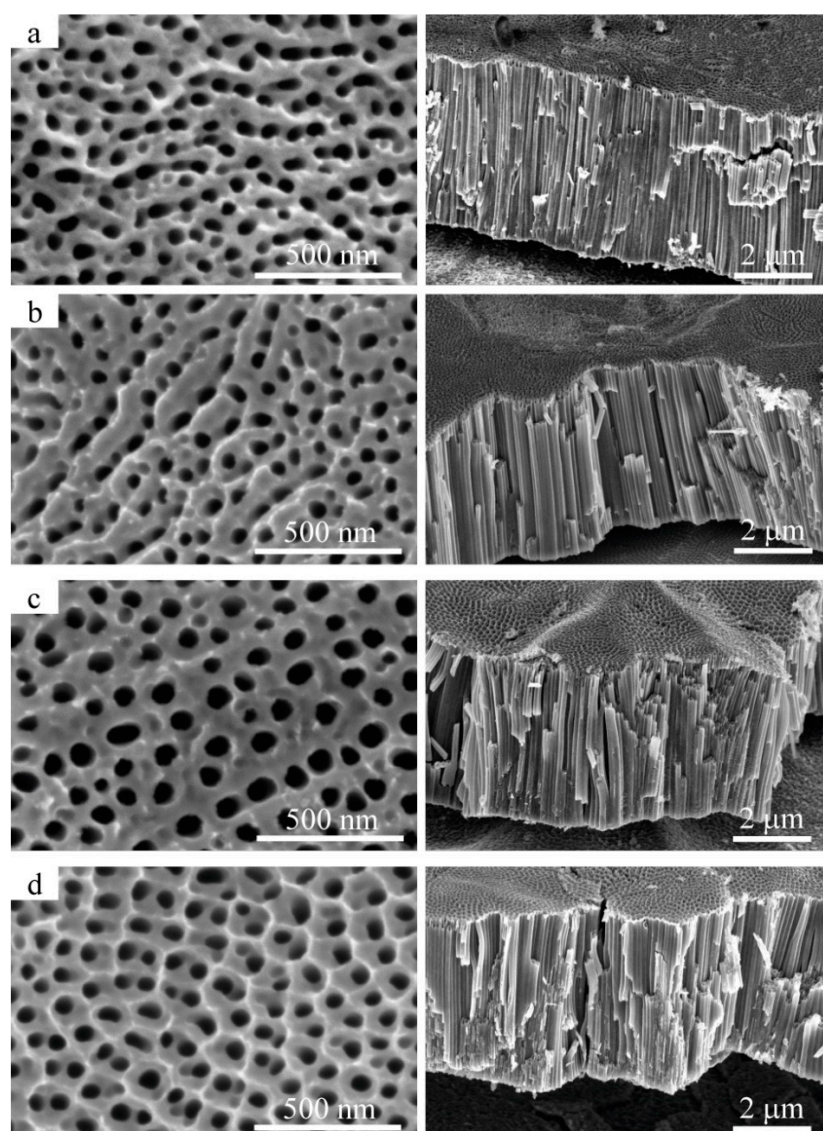
Figure 2. SEM images of symmetric TiO_2 nanotube arrays top and cross-section view: Air 450 (**a**), Arg 300 (**b**), Arg 400 (**c**), and Arg 550 (**d**).

Table 1. The composition of obtained samples TiO_2 NTs arrays annealed in different conditions.

Sample	Ti, at.%	O, at.%	C, at.%	N, at.%	F, at.%
Air 450	33.0	62.0	4.6	0	0
Arg 300	24.6	55.4	11.2	2.0	6.2
Arg 400	26.9	61.2	8.9	2.2	0.3
Arg 550	30.0	64.0	5.0	0	0.1

As can be seen, the ratio of atoms of Ti to oxygen in the Air 450 sample is close to 1:2, at the same time the presence of carbon on the surface of the sample of 4.6 at.% was recorded. Most of the carbon can be associated with adsorbed organic compounds from the atmosphere. At the same time, for samples Arg 300 and Arg 400, we can observe an increased amount of carbon (above the background value of the adsorbed organic compounds), 11.2 and 8.9 at.%, respectively. It is expected that increasing the temperature of thermal treatment in argon leads to a decrease in the amount of carbon in the material. It can be noticed that for the Arg 550 sample the amount of carbon exceeds the background

value by ~0.4%, but we cannot say for sure that this difference is not a measurement error. It should also be noted, the presence of a significant amount of fluorine in the sample Arg 300, its presence is due to the use of fluorine-containing electrolyte during anodizing. Nitrogen was detected in samples Arg 300 and Arg 400, its presence can also be explained by the composition of the electrolyte. The presence of nitrogen in these samples may affect their photoactivity in the visible light range, according to [33,34].

The crystal structure of the obtained samples was studied by X-ray diffraction analysis (Figure 3). Ti foil without oxide was used as a comparison sample.
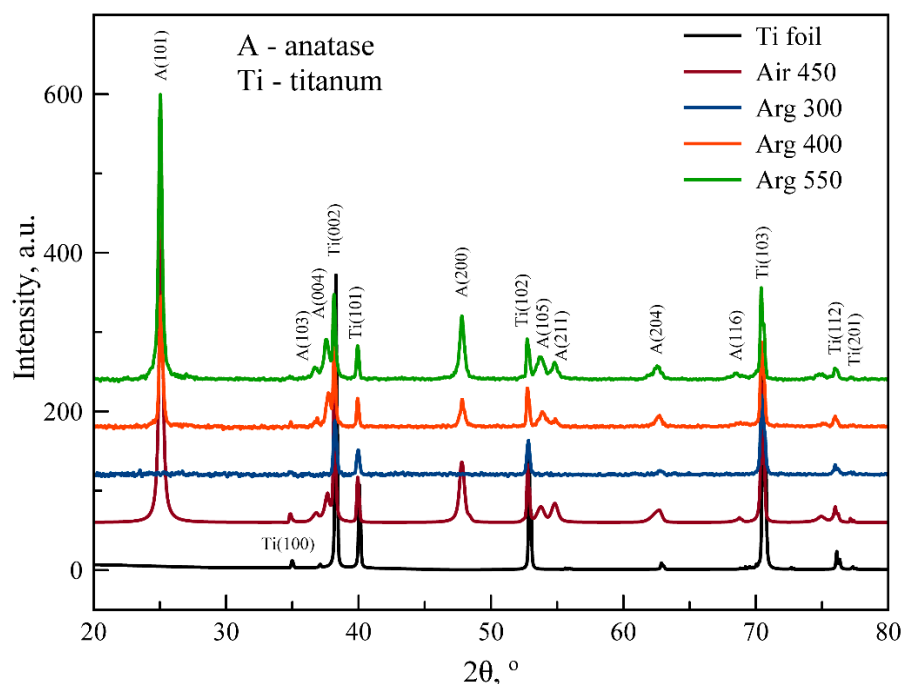

Figure 3. XRD analysis of annealed in argon samples at different temperatures and references (Ti foil without oxide layer and annealed symmetric TiO_2-NTs on air).

All registered peaks could be clearly attributed to the characteristic peaks of TiO_2 anatase and titanium (JCPDS-ICDD: 21-1272 and JCPDS-ICDD: 44-1294 correspondingly). The diffraction peaks of TiO_2 anatase at about 2θ of 25.05, 36.7, 37.58, 47.81, 53.81, 54.82, 62.6, and 62.9 correspond to the orientations (101), (103), (004), (200), (105), (211), (204), and (216), respectively. The results show that the sample crystallization does not occur during annealing at 300 °C, which correlates with the DSC data obtained. At the same time, we can note that the intensity of the anatase peaks for the Arg 400 sample is less than for Arg 550, which may indicate a lower degree of ordering of the Arg 400 sample structure. Despite the high annealing temperature, no rutile phase was detected in sample Arg 550.

Raman spectra are shown in Figure 4. For all samples except amorphous TiO_2 NTs (as-prepared) and Arg 300, the main peak of the anatase phase (146 cm^{-1}) can be observed.

It can be seen that the spectrum of samples that were thermally treated in an argon stream is distorted by photoluminescence. As the thermal treatment temperature increases to 400 °C, the photoluminescence increases. This effect can be attributed to oxygen vacancies or carbon content formed in the nanostructure during thermal treatment in an inert argon atmosphere [35]. Additionally, nitrogen in the TiO_2 matrix can lead to a fluorescence effect [36]. In spite of the noisiness of the spectrum, the peak with a maximum at 1570 cm^{-1} can observe for both Arg 300 and Arg 400 samples. This peak can be associated with carbon in the sp2 hybridization state (G bond) and based on the shape of the peak, carbon is in an amorphous state [37]. In the Arg 550 sample, photoluminescence was observed to a lesser extent, and the main peaks of polymorphic modification of anatase were recorded at 146, 398, 520, and 637 cm^{-1} as for the Air 450 sample. As the concentration of carbon

and nitrogen in the Arg 550 sample nanostructure decreases compared to Arg 400, the photoluminescence intensity decreases. A decrease in the content of carbon and nitrogen can lead to a decrease in the contribution of radiative recombination and, consequently, in the intensity of photoluminescence. It is worth noting that photoluminescence is not observed in the sample thermally treated in air.
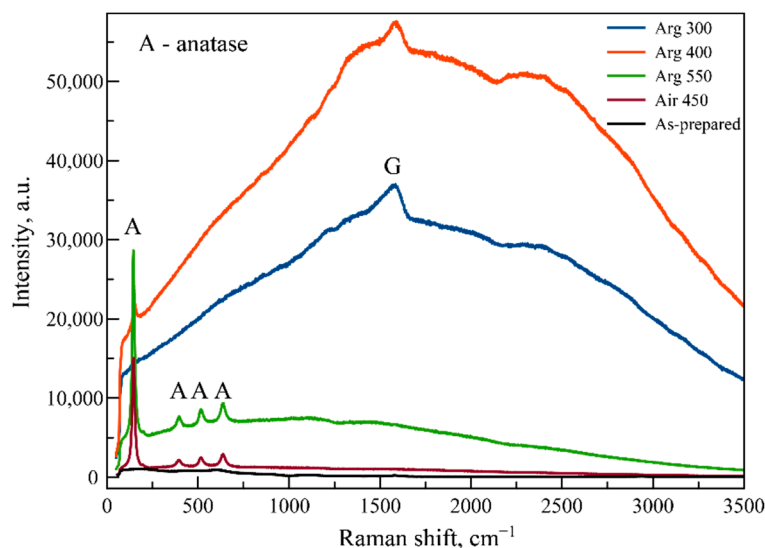

Figure 4. Raman shift spectra of the obtained samples annealed in argon.

Registered carbon also can be associated with carbon dangling bonds. Such carbon bonds can accumulate an excess negative charge, thereby contributing to greater photocatalytic activity during CO_2 conversion [31,38].

3.3. Functional Properties Investigation

The optical properties of the obtained samples were investigated by diffuse light reflectance spectroscopy (Figure 5). It can be seen that the reflection coefficient in the range from 300 to 650 nm decreases with annealing temperature in an argon stream (Figure 5a). The Arg 300 sample has the lowest reflection coefficient in the entire measured range, but due to the fact that no symmetric crystal structure is observed, such a sample cannot be used as a photocatalyst or photoanode. The reflection coefficient increases with the temperature of thermal treatment in an argon stream (Figure 5a). The obtained spectra of diffuse light reflection were recalculated according to the Kubelka–Munk theory (Figure 5b). The values of the optical band gap width of the obtained samples were determined. The band gap width of Arg 300 and Arg 400 samples is close and is about 2.9 eV, in turn for Arg 550 and Air 450 samples, it is about 3.1 eV. A little decrease in the optical bandgap width of Arg 300 and Arg 400 samples compared to Arg 550 and Air 450 can be attributed to the presence of carbon and nitrogen in the material [36,39].

Figure 6 shows the voltammetric characteristics of the symmetric TiO_2-NTs in darkness, under illumination by the xenon lamp (full spectrum) and under illumination with a wavelength of more than 430 nm.

As can be seen, the Arg 300 sample shows no photoactivity in any of the emission spectra. This is due to the amorphous structure of the sample, leading to a large degree of recombination of photogenerated charge carriers in the volume of the material. It can be seen that the samples Air 450 and Arg 550 have the highest photoactivity in the full spectrum, the maximum photocurrent recorded during the measurement at 0.5 V was 0.6 and 0.4 mA/cm^2, respectively. At the same time, the Arg 400 sample shows low photoactivity in the full spectrum with a maximum photocurrent at 1 V of about 0.25 mA/cm^2.
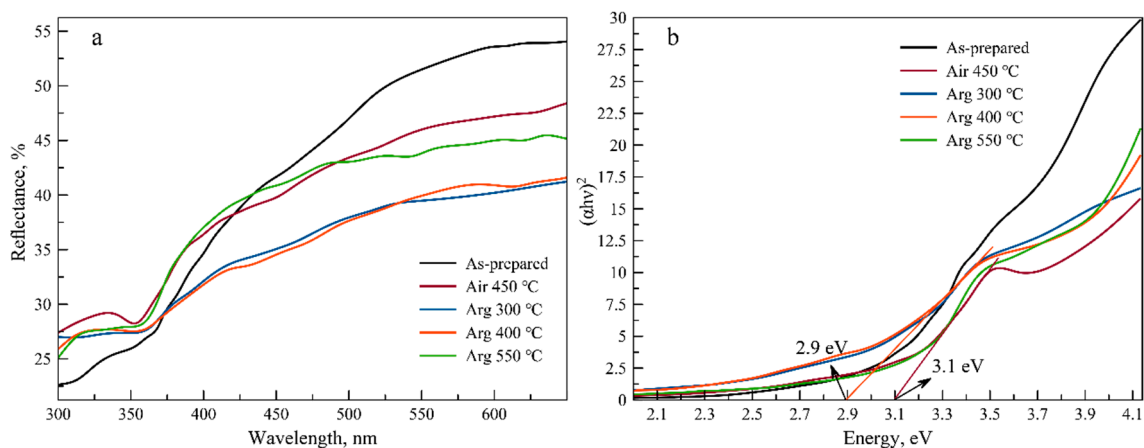
Figure 5. DRS spectra (**a**) and determination of the band gap for the samples according to the Kubelka–Munch theory (**b**).
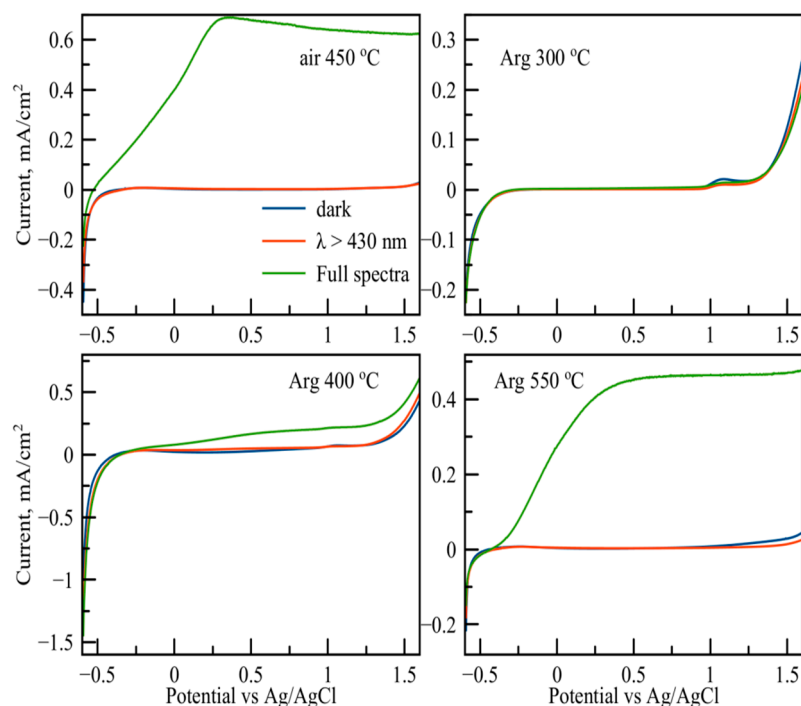

Figure 6. Voltammetric characteristics of the symmetric TiO_2-NTs under different conditions of illumination.

The photoactivity of the samples was also investigated by chronoamperometry under visible light and full spectra at 0 V bias vs. Ag/AgCl (Figure 7).

As can be seen from obtained data, the Arg 400 sample has the highest photoactivity in the visible light range, its registered values of photocurrent exceed other samples by at least 15 times. That correlates with the optic band gap measurements, the band gap of the Arg 300 is lower than the Air 450 and Arg 550 samples. However, the overall photoactivity of light conversion of the Arg 400 sample in the full spectrum is low. This effect may be related to the high defectiveness of the structure due to excessive carbon and nitrogen content in the material. Increasing the annealing temperature in argon to 550 °C and the decrease in carbon and nitrogen content leads to an increase in the photoactivity of the material in full spectra of the xenon lamp. However, when compared to the Air 450 sample, the effect of thermal treatment in an argon stream on the photoactivity of the samples is negative.
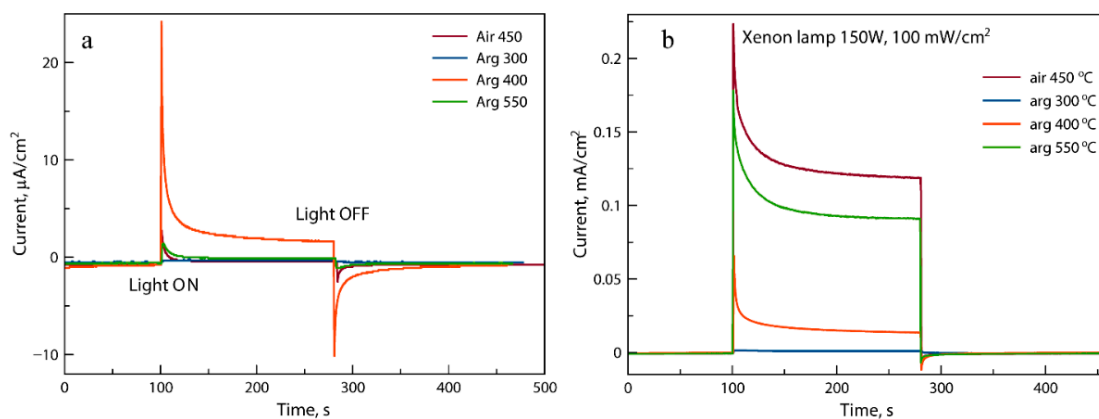
Figure 7. Photocurrent transients of TiO_2 NTs samples under different illumination spectra: visible light (**a**), full spectra (**b**).

The light conversion efficiency of obtained samples was evaluated in the wavelength range of 300 to 500 nm at an applied 0 V bias vs. Ag/AgCl (Figure 8).
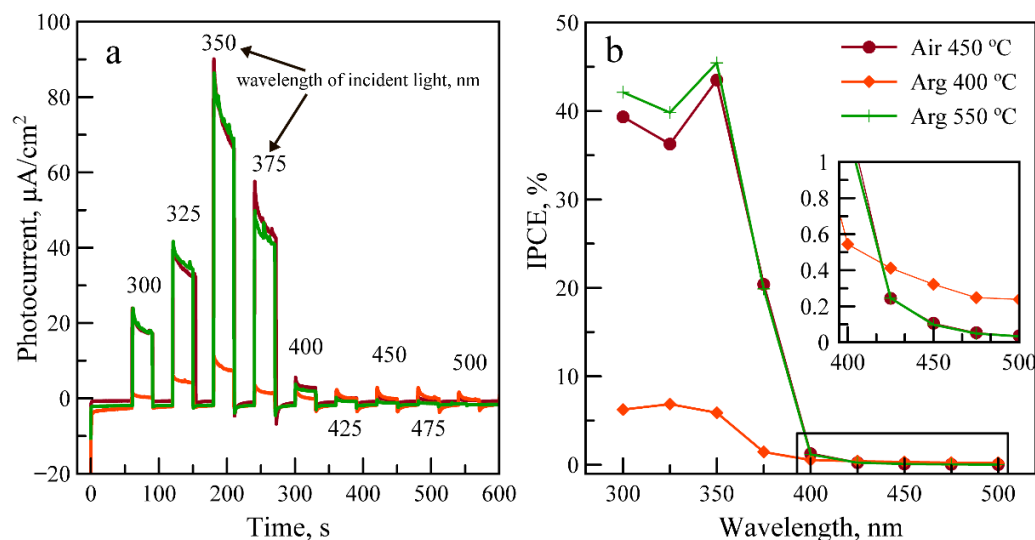

Figure 8. Photocurrent transients under different illumination spectra (**a**) and calculated IPCE (**b**) data at applied 0 V bias vs. Ag/AgCl.

As can be seen, Air 450 and Arg 550 samples most effectively convert light at wavelengths less than 400 nm. At the same time, the Arg 400 sample showed less than 10% light conversion efficiency in the entire range studied. The low light conversion efficiency of the Arg 400 sample can be associated with light adsorption by amorphous surface carbon without generation charge carriers. One can notice a light conversion efficiency of ~0.2% at wavelengths longer than 400 nm probably because of the fast recombination of generated charge carriers (Figure 8).

The process of photocatalytic conversion of CO_2 was carried out in a flow-through reactor with a gas flow rate of 1.1 mL·min^{-1}. The obtained results are presented in Figure 9. As can be seen in Figure 9, the release of methane and methanol occurs when the light is turned on in the stream of wet helium. Products such as acetaldehyde and ethanol have also been detected. The presence of these products in the wet helium stream with light irradiation can be associated with two symmetric processes: photocatalytic decomposition of adsorbed organic compounds on the surface of the symmetric TiO_2 NTs, as well as desorption of such compounds. After the system was stabilized, the working gas was changed to CO_2 without changing the gas flow rate. The concentration of methanol and

methane increases with the presence of CO_2 in the reactor for all studied samples. This effect indicates the beginning of the photocatalytic conversion of CO_2.
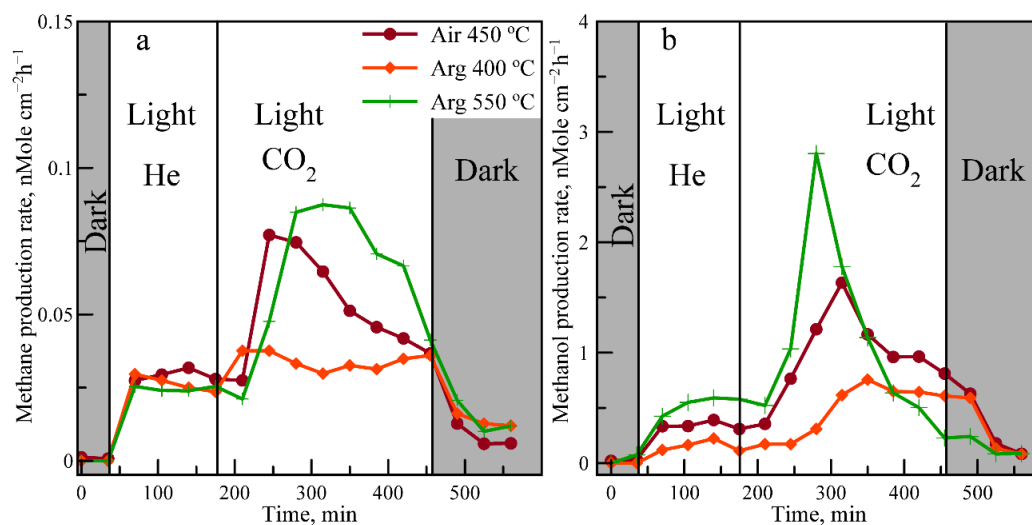

Figure 9. Kinetics of photocatalytic CO_2 conversion process to methane (**a**) and methanol (**b**).

It can be noted that the yield of methane and methanol in the helium stream for all samples under investigation is not much different, which can indicate that the carbon on the surface of the material is not converted into organic compounds. Methane and methanol are common CO_2 conversion products for TiO_2-based photocatalysts [4]. As can be seen, the greatest photocatalytic activity exhibits the sample Arg 550, but after 120 min of the CO_2 injection in the reaction the rate of photoconversion critically decreases. The activity of Arg 550 rapidly decreases during the formation of methanol, to almost zero even before the light is turned off. That can indicate the active deactivation of the photocatalyst surface. The deactivation can be connected with adsorbed reaction products on the sample's surface and further block the photocatalytic process. At the same time, for sample Air 450, the decrease in the production rate of methanol can be observed, but to a lesser extent compared to Arg 550. The Arg 400 sample has the lowest photocatalytic activity, but it should be noted that during 440 min of photoinduced conversion of CO_2, deactivation of the photocatalyst is not observed.

The photocatalytic activity of the Arg 550 sample is higher than that of the Air 450 sample, which can be explained by the large number of carbon dangling bonds that accumulate an excess negative charge. However, as can be assumed such carbon defects are not stable and are quickly deactivated in the CO_2 conversion process by the reaction products, which is observed in these two samples. In turn, the Arg 400 sample with the greatest amount of carbon in its composition shows a low production rate but stable kinetics of methane and methanol formation during experiment time. We can assume two symmetric processes: the surface carbon is a drain for the electrons from carbon dangling bonds, and the CO_2 conversion process takes place at a distance from such carbon centers, due to which their passivation does not occur.

As can be seen from the obtained results the excess modification by carbon of TiO_2 nanotube arrays leads to a decrease in the photocatalytic activity in the CO_2 conversion process. The presence of carbon dangling bonds increases the rate of the CO_2 conversion process, but their amount should be optimal. Controlling the concentration of such carbon centers can be a good way to obtain an efficient catalyst in carbon dioxide conversion processes. In the case of the photoanode material, excessive carbon doping leads to an increase in photoactivity in the visible range, but critically suppresses the light conversion in the UV range.

4. Conclusions

In the present work, we have investigated the influence of the temperature of thermal treatment in argon on the structure, chemical, and phase composition, as well as photocatalytic and photoelectrochemical properties of arrays of the symmetric titanium oxide nanotubes obtained in ethylene glycol-based electrolyte. It can be concluded that thermal treatment of the symmetric TiO_2 NTs in argon contributes to the preservation of carbon in the material. Carbon modification of the symmetric TiO_2 NTs arrays leads to an increase in optical absorption in the visible light range. In turn, carbon modification of the symmetric TiO_2 NTs arrays promotes the process of CO_2 conversion. This effect may be related to the formation of carbon dangling bonds in the structure of the samples. Such defects accumulate electrons on the surface required for the carbon dioxide conversion reaction. However, despite the increased activity of such carbon defects, they seem to be prone to passivation. At the same time, the presence of carbon in the samples is necessary because it leads to greater stability of the CO_2 conversion process, which may be a consequence of the separation of photoinduced charge carriers on the catalyst surface. Further development of methods to control the concentration of carbon dangling bonds and protect them from deactivation may be a successful way to increase the activity of the symmetric TiO_2 NTs arrays in the photocatalytic conversion of CO_2.

Author Contributions: Conceptualization, T.S. and A.D.; methodology, A.D.; software, A.T.; validation, T.S., I.G. and A.D.; formal analysis, T.S.; investigation, A.S., D.D. and S.P.; data curation, I.G.; writing—original draft preparation, T.S. and I.G.; writing—review and editing, E.K.; visualization, T.M.; supervision, S.G. All authors have read and agreed to the published version of the manuscript.

Data Availability Statement: The datasets obtained and analyzed during the current study are available from the corresponding author upon reasonable request.

Conflicts of Interest: The authors declare no conflict of interest. The funders had no role in the design of the study; in the collection, analyses, or interpretation of data; in the writing of the manuscript, or in the decision to publish the results.

References

1. Takht Ravanchi, M.; Sahebdelfar, S. Catalytic Conversions of CO_2 to Help Mitigate Climate Change: Recent Process Developments. *Process Saf. Environ. Prot.* **2021**, *145*, 172–194. [CrossRef]
2. Fu, J.; Jiang, K.; Qiu, X.; Yu, J.; Liu, M. Product Selectivity of Photocatalytic CO2 Reduction Reactions. *Mater. Today* **2020**, *32*, 222–243. [CrossRef]
3. Jiang, Y.; Wang, Y.; Zhang, Z.; Dong, Z.; Xu, J. 2D/2D $CsPbBr_3$/BiOCl Heterojunction with an S-Scheme Charge Transfer for Boosting the Photocatalytic Conversion of CO_2. *Inorg. Chem.* **2022**, *61*, 10557–10566. [CrossRef] [PubMed]
4. Barrocas, B.T.; Ambrožová, N.; Kočí, K. Photocatalytic Reduction of Carbon Dioxide on TiO_2 Heterojunction Photocatalysts—A Review. *Materials* **2022**, *15*, 967. [CrossRef]
5. Domínguez-Espíndola, R.B.; Arias, D.M.; Rodríguez-González, C.; Sebastian, P.J. A Critical Review on Advances in TiO_2-Based Photocatalytic Systems for CO_2 Reduction. *Appl. Therm. Eng.* **2022**, *216*, 119009. [CrossRef]
6. Wang, J.; Guo, R.T.; Bi, Z.X.; Chen, X.; Hu, X.; Pan, W.G. A Review on TiO_{2-x}-Based Materials for Photocatalytic CO_2 Reduction. *Nanoscale* **2022**, *14*, 11512–11528. [CrossRef]
7. Palmas, S.; Mais, L.; Mascia, M.; Vacca, A. Trend in Using TiO_2 Nanotubes as Photoelectrodes in PEC Processes for Wastewater Treatment. *Curr. Opin. Electrochem.* **2021**, *28*, 100699. [CrossRef]
8. Feng, Y.; Rijnaarts, H.H.M.; Yntema, D.; Gong, Z.; Dionysiou, D.D.; Cao, Z.; Miao, S.; Chen, Y.; Ye, Y.; Wang, Y. Applications of Anodized TiO_2 Nanotube Arrays on the Removal of Aqueous Contaminants of Emerging Concern: A Review. *Water Res.* **2020**, *186*, 116327. [CrossRef]
9. Grabowska, E.; Marchelek, M.; Klimczuk, T.; Trykowski, G.; Zaleska-Medynska, A. Noble Metal Modified TiO_2 Microspheres: Surface Properties and Photocatalytic Activity under UV–Vis and Visible Light. *J. Mol. Catal. A Chem.* **2016**, *423*, 191–206. [CrossRef]

10. Enachi, M.; Guix, M.; Braniste, T.; Postolache, V.; Ciobanu, V.; Ursaki, V.; Schmidt, O.G.; Tiginyanu, I. Photocatalytic Properties of TiO2 Nanotubes Doped with Ag, Au and Pt or Covered by Ag, Au and Pt Nanodots. *Surf. Eng. Appl. Electrochem.* **2015**, *51*, 3–8. [CrossRef]

11. Wang, X.; Sun, M.; Murugananthan, M.; Zhang, Y.; Zhang, L. Electrochemically Self-Doped WO_3/TiO_2 Nanotubes for Photocatalytic Degradation of Volatile Organic Compounds. *Appl. Catal. B Environ.* **2020**, *260*, 118205. [CrossRef]

12. Rimoldi, L.; Giordana, A.; Cerrato, G.; Falletta, E.; Meroni, D. Insights on the Photocatalytic Degradation Processes Supported by TiO_2/WO_3 Systems. The Case of Ethanol and Tetracycline. *Catal. Today* **2019**, *328*, 210–215. [CrossRef]

13. Zhang, Q.; Zheng, D.D.; Xu, L.S.; Chang, C.T. Photocatalytic Conversion of Terephthalic Acid Preparation Wastewater to Hydrogen by Graphene-Modified TiO_2. *Catal. Today* **2016**, *274*, 8–14. [CrossRef]

14. Masoud, M.; Nourbakhsh, A.; Hassanzadeh-Tabrizi, S.A. Influence of Modified CNT-Ag Nanocomposite Addition on Photocatalytic Degradation of Methyl Orange by Mesoporous TiO_2. *Inorg. Nano-Metal Chem.* **2017**, *47*, 1168–1174. [CrossRef]

15. Naldoni, A.; Altomare, M.; Zoppellaro, G.; Liu, N.; Kment, Š.; Zbořil, R.; Schmuki, P. Photocatalysis with Reduced TiO_2: From Black TiO_2 to Cocatalyst-Free Hydrogen Production. *ACS Catal.* **2019**, *9*, 345–364. [CrossRef] [PubMed]

16. Dong, Z.; Zhang, Z.; Jiang, Y.; Chu, Y.; Xu, J. Embedding CsPbBr3 Perovskite Quantum Dots into Mesoporous TiO2 Beads as an S-Scheme Heterojunction for CO_2 Photoreduction. *Chem. Eng. J.* **2022**, *433*, 133762. [CrossRef]

17. Dong, Z.; Zhou, J.; Zhang, Z.; Jiang, Y.; Zhou, R.; Yao, C. Construction of a P-n Type S-Scheme Heterojunction by Incorporating $CsPbBr_3$Nanocrystals into Mesoporous Cu_2O Microspheres for Efficient CO2Photoreduction. *ACS Appl. Energy Mater.* **2022**, *5*, 10076–10085. [CrossRef]

18. Mohamed, A.E.R.; Barghi, S.; Rohani, S. N- and C-Modified TiO_2 Nanotube Arrays: Enhanced Photoelectrochemical Properties and Effect of Nanotubes Length on Photoconversion Efficiency. *Nanomaterials* **2018**, *8*, 198. [CrossRef]

19. Shin, S.W.; Lee, J.Y.; Ahn, K.S.; Kang, S.H.; Kim, J.H. Visible Light Absorbing TiO_2 Nanotube Arrays by Sulfur Treatment for Photoelectrochemical Water Splitting. *J. Phys. Chem. C* **2015**, *119*, 13375–13383. [CrossRef]

20. Saud, P.S.; Pant, B.; Alam, A.M.; Ghouri, Z.K.; Park, M.; Kim, H.Y. Carbon Quantum Dots Anchored TiO2 Nanofibers: Effective Photocatalyst for Waste Water Treatment. *Ceram. Int.* **2015**, *41*, 11953–11959. [CrossRef]

21. Savchuk, T.; Yakubov, A.; Gavrilin, I.; Dronova, D.; Dronov, A. Influence of Thermal Post-Treatment on Electrophysical Properties of Carbon Modified Anodic TiO_2 NTs. In Proceedings of the 2019 IEEE Conference of Russian Young Researchers in Electrical and Electronic Engineering (EIConRus), Saint Petersburg and Moscow, Moscow, Russia, 28–31 January 2019; pp. 1970–1972. [CrossRef]

22. Matos, J.; García, A.; Zhao, L.; Titirici, M.M. Solvothermal Carbon-Doped TiO_2 Photocatalyst for the Enhanced Methylene Blue Degradation under Visible Light. *Appl. Catal. A Gen.* **2010**, *390*, 175–182. [CrossRef]

23. Shao, J.; Sheng, W.; Wang, M.; Li, S.; Chen, J.; Zhang, Y.; Cao, S. In Situ Synthesis of Carbon-Doped TiO_2 Single-Crystal Nanorods with a Remarkably Photocatalytic Efficiency. *Appl. Catal. B Environ.* **2017**, *209*, 311–319. [CrossRef]

24. Hua, L.; Yin, Z.; Cao, S. Recent Advances in Synthesis and Applications of Carbon-Doped TiO_2 Nanomaterials. *Catalysts* **2020**, *10*, 1431. [CrossRef]

25. Gao, Z.D.; Zhu, X.; Li, Y.H.; Zhou, X.; Song, Y.Y.; Schmuki, P. Carbon Cladded TiO_2 Nanotubes: Fabrication and Use in 3D-RuO2 Based Supercapacitors. *Chem. Commun.* **2015**, *51*, 7614–7617. [CrossRef] [PubMed]

26. Hu, L.; Huo, K.; Chen, R.; Gao, B.; Fu, J.; Chu, P.K. Recyclable and High-Sensitivity Electrochemical Biosensing Platform Composed of Carbon-Doped TiO_2 Nanotube Arrays. *Anal. Chem.* **2011**, *83*, 8138–8144. [CrossRef]

27. Song, Y.Y.; Li, Y.H.; Guo, J.; Gao, Z.D.; Li, Y. Facile Method to Synthesize a Carbon Layer Embedded into Titanium Dioxide Nanotubes with Metal Oxide Decoration for Electrochemical Applications. *J. Mater. Chem. A* **2015**, *3*, 23754–23759. [CrossRef]

28. Chen, B.; Haring, A.J.; Beach, J.A.; Li, M.; Doucette, G.S.; Morris, A.J.; Moore, R.B.; Priya, S. Visible Light Induced Photocatalytic Activity of Fe^{3+}/Ti^{3+} Co-Doped TiO_2 Nanostructures. *RSC Adv.* **2014**, *4*, 18033–18037. [CrossRef]

29. Gavrilin, I.; Dronov, A.; Volkov, R.; Savchuk, T.; Dronova, D.; Borgardt, N.; Pavlikov, A.; Gavrilov, S.; Gromov, D. Differences in the Local Structure and Composition of Anodic TiO2 Nanotubes Annealed in Vacuum and Air. *Appl. Surf. Sci.* **2020**, *516*, 146120. [CrossRef]

30. Dronov, A.; Gavrilin, I.; Kirilenko, E.; Dronova, D.; Gavrilov, S. Investigation of Anodic TiO_2 Nanotube Composition with High Spatial Resolution AES and ToF SIMS. *Appl. Surf. Sci.* **2018**, *434*, 148–154. [CrossRef]

31. Savchuk, T.; Gavrilin, I.; Konstantinova, E.; Dronov, A.; Volkov, R.; Borgardt, N.; Maniecki, T.; Gavrilov, S.; Zaitsev, V. Anodic TiO_2 nanotube Arrays for Photocatalytic CO_2 conversion: Comparative Photocatalysis and EPR Study. *Nanotechnology* **2022**, *33*, 055706. [CrossRef]

32. Varghese, O.K.; Grimes, C.A. Appropriate Strategies for Determining the Photoconversion Efficiency of Water Photoelectrolysis Cells: A Review with Examples Using Titania Nanotube Array Photoanodes. *Sol. Energy Mater. Sol. Cells* **2008**, *92*, 374–384. [CrossRef]

33. Khan, T.T.; Rafiqul Bari, G.A.K.M.; Kang, H.J.; Lee, T.G.; Park, J.W.; Hwang, H.J.; Hossain, S.M.; Mun, J.S.; Suzuki, N.; Fujishima, A.; et al. Synthesis of N-Doped TiO_2 for Efficient Photocatalytic Degradation of Atmospheric NO_x. *Catalysts* **2021**, *11*, 109. [CrossRef]

34. Huang, J.; Dou, L.; Li, J.; Zhong, J.; Li, M.; Wang, T. Excellent Visible Light Responsive Photocatalytic Behavior of N-Doped TiO2 toward Decontamination of Organic Pollutants. *J. Hazard. Mater.* **2021**, *403*, 123857. [CrossRef] [PubMed]

35. Blasco-Tamarit, E.; Solsona, B.; Sánchez-Tovar, R.; García-García, D.; Fernández-Domene, R.M.; García-Antón, J. Influence of Annealing Atmosphere on Photoelectrochemical Response of TiO$_2$ Nanotubes Anodized under Controlled Hydrodynamic Conditions. *J. Electroanal. Chem.* **2021**, *897*, 115579. [CrossRef]
36. Pérez, E.; Torres, M.F.; Morales, G.; Murgia, V.; Sham, E. Synthesis of N-TiO$_2$ Effect of the Concentration of Nitrogen in the Band Gap. *Procedia Mater. Sci.* **2015**, *8*, 649–655. [CrossRef]
37. Ferrari, A.C.; Robertson, J. Resonant Raman Spectroscopy of Disordered, Amorphous, and Diamondlike Carbon. *Phys. Rev. B Condens. Matter Mater. Phys.* **2001**, *64*, 075414. [CrossRef]
38. Konstantinova, E.A.; Kytina, E.V.; Zaitsev, V.B.; Martyshov, M.N.; Savchuk, T.P.; Kamaleev, M.F. Photoelectron Properties of Multi-Walled and Single-Walled Titania a Nanotubes. *Russ. J. Phys. Chem. B* **2022**, *16*, 797–803. [CrossRef]
39. Kwak, C.H.; Im, U.S.; Seo, S.W.; Kim, M., II; Huh, Y.S.; Im, J.S. Effects of Carbon Doping on TiO2 for Enhanced Visible Light-Driven NO Sensing Performance. *Mater. Lett.* **2021**, *288*, 129313. [CrossRef]